Veterinary Microbiology xxx (xxxx) 109024

Contents lists available at ScienceDirect

Veterinary Microbiology

journal homepage: www.elsevier.com/locate/vetmic

Stem II-disrupting pseudoknot does not abolish ability of Senecavirus A IRES to initiate protein expression, but inhibits recovery of virus from cDNA clone

Fuxiao Liu [1], **, Ning Wang [1], Yilan Huang, Qianqian Wang, Hu Shan *

College of Veterinary Medicine, Qingdao Agricultural University, Qingdao, 266109, China

ARTICLE INFO

Keywords:
Senecavirus A
Internal ribosome entry site
Pseudoknot
Minigenome
Mutation
Rescue

ABSTRACT

Senecavirus A (SVA) is classified into the genus *Senecavirus* in the family *Picornaviridae*. Its genome is a positive-sense, single-stranded and nonsegmented RNA, approximately 7300 nucleotides in length. A picornaviral genome is essentially an mRNA, which, albeit unmodified with 5′ cap structure, can still initiate protein expression by the internal ribosome entry site (IRES). The SVA genome contains a hepatitis C virus-like IRES, in which a pseudoknot structure plays an important role in initiating protein expression. In this study, we constructed a set of SVA (CH-LX-01-2016 strain) minigenomes with all combinations of point mutations in its pseudoknot stem II (PKS-II). The results showed that any combination of point mutations could not significantly interfere with the IRES to initiate protein expression. Further, we constructed a full-length SVA cDNA clone, in which the PKS-II-forming cDNA motif was subjected to site-directed mutagenesis for totally disrupting the PKS-II formation in IRES. Such a modified SVA cDNA clone was transfected into BSR-T7/5 cells, consequently demonstrating that the PKS-II-disrupting IRES interfered neither with protein expression nor with antigenome replication, whereas a competent SVA could not be rescued from the cDNA clone. It was speculated that the mutated motif possibly disrupted a packaging signal for virion assembly, therefore causing the failure of SVA rescue.

1. Introduction

Senecavirus A (SVA), also known as Seneca Valley virus (SVV), belongs to the genus *Senecavirus* in the family *Picornaviridae*. SVA is an emerging virus that causes vesicular disease in pigs, whose clinical signs are indistinguishable from those caused by foot-and-mouth disease virus (Liu et al., 2020b). Some herds additionally suffer an increase in neonatal losses of 1- to 4-day-old piglets (Houston et al., 2020). This virus is not pathogenic to normal human cells, but has potent oncolytic activity in tumor cells, such as neuroendocrine tumor cells (Liu et al., 2021b; Reddy et al., 2007) and human retinoblastoma cells (Wadhwa et al., 2007). The SVA genome is a positive-sense, single-stranded, nonsegmented and linear RNA, approximately 7300 nt in length, with a 3′ poly (A) tail but without a 5′ capped structure. The genome contains 5′ and 3′ untranslated regions (UTR), and a single long open reading frame (ORF) of polyprotein precursor.

The 5′ UTR contains a sequence of hepatitis C virus (HCV)-like internal ribosome entry site (IRES) (Martínez-Salas et al., 2015), allowing for translation initiation in a cap-independent manner. The 3′ UTR reveals a kissing-loop structure, followed by a poly (A) sequence. The polyprotein ORF follows the standard "L–VP4–VP2–VP3–VP1–2A–2B–2C–3A–3B–3C–3D" layout (Hales et al., 2008). Referring to other picornaviruses (McKnight and Lemon, 2018; Sun et al., 2016; Wang and Li, 2019), the VP1, VP2, VP3 and VP4 are four structural proteins, required for encapsidation of SVA genome. The 2A performs the function of ribosomal skipping. The 2C protein is a helicase-like polypeptide involved in RNA synthesis. The 3B (VPg) is a genome-linked polypeptide, functioning as a protein primer for RNA synthesis. The 3C ($3C^{pro}$) is a protease, responsible for cleaving the SVA polyprotein precursor. The 3D ($3D^{pol}$) is a RNA-dependent RNA polymerase, functioning in virus replication and VPg uridylylation.

A picornaviral genome is actually an mRNA, which, albeit unmodified with 5′ cap structure, can still initiate protein expression by the IRES that recruits ribosomal subunits using a process independent of the cap-binding protein, eukaryotic initiation factor (eIF) 4E. The picornaviral IRES was initially reported in genomes of poliovirus (Pelletier

* Corresponding author.
** Corresponding author.
E-mail addresses: laudawn@126.com (F. Liu), shanhu67@163.com (H. Shan).
[1] The contribution is equal to this work.

https://doi.org/10.1016/j.vetmic.2021.109024
Received 9 December 2020; Accepted 26 February 2021
0378-1135/

and Sonenberg, 1988) and encephalomyocarditis virus (Jang et al., 1988), and subsequent studies demonstrated that different types of IRES elements could drive internal initiation of translation from mRNAs of all picornaviral members (Martínez-Salas et al., 2015). Based on RNA secondary structure, the picornaviral IRES elements are generally classified into five types, namely type I, II, III, HCV-like and aichivirus (AV)-like (Lozano and Martínez-Salas, 2015). The picornaviral HCV-like IRES was initially identified in the genome of porcine teschovirus-1 (PTV-1) (Kaku et al., 2002), and subsequently found in numerous members in the family *Picornaviridae* (Chard et al., 2006a), such as avian encephalomyelitis virus (Bakhshesh et al., 2008) and SVA (Willcocks et al., 2011).

RNA pseudoknots are structural elements, existing in almost all classes of RNA. A pseudoknot is a structure formed upon base-pairing of a single-stranded region of RNA in the loop of a hairpin to a stretch of complementary nucleotides elsewhere in the RNA chain (Brierley et al., 2007). The HCV-like IRES forms a defined secondary structure that contains two major hairpins, termed domain II and III (Chard et al., 2006b; Easton et al., 2009). Initial binding of the 40S ribosomal subunit is mediated mainly by the basal region of domain III, including the stem-loop IIId, with a modest contribution from an H-type pseudoknot upstream of the start codon (Kieft et al., 2001; Otto and Puglisi, 2004). The pseudoknot consists of two base-paired stem regions (stem I and II) connected by two loops, the stem sequences are not especially well conserved, but the presence of the structure is highly conserved with compensatory base changes that preserve the base-pairing (Belsham, 2009). A proposed model showed that different domains in an HCV IRES functioned synergistically to position the start codon into the ribosomal P site, coupled to movement of the pseudoknot that was upstream of the start codon (Boehringer et al., 2005).

The pseudoknot has been demonstrated to be critical for the activity of picornaviral HCV-like IRESs (Bakhshesh et al., 2008; Chard et al., 2006b; Pan et al., 2012; Willcocks et al., 2011). For instance, structural disruption of the pseudoknot in the stem, either I or II, of PTV-1 caused significant inactivity of its IRES to initiate protein expression (Chard et al., 2006b). As to SVA (SVV-001 strain), the activity of IRES could even be totally attenuated by only two point mutations in the pseudoknot stem II (PKS-II) (Willcocks et al., 2011). The SVA PKS-II is predicted to be a 5-base-paired stem structure, containing a non-Watson–Crick base pair, G:U base pair. Contrary to the conclusion in the literature (Willcocks et al., 2011), we demonstrated that any combination of point mutations in SVA (CH-LX-01-2016 strain) PKS-II could not significantly interfere with the IRES activity. The SVA PKS-II formation, if completely disrupted, was shown to have no significant impact on the replication of SVA antigenome, but to inhibit recovery of competent SVA from a cDNA clone that contained a 5-nt-mutated motif in the PKS-II.

2. Materials and methods

2.1. Cell line and plasmids

The T7 RNA polymerase-expressing BHK (BSR-T7/5) cells (Buchholz et al., 1999) were cultured at 37 °C with 5% CO_2 in Dulbecco's modified Eagle's medium (DMEM), supplemented with 10 % fetal bovine serum (FBS) and G418 (500 μg/mL). The pUC57 plasmid was used for constructing a SVA minigenome. The full-length SVA cDNA clone, used for rescuing the enhanced green fluorescent protein (eGFP)-tagged recombinant SVA (rSVA-eGFP), was constructed previously in our laboratory (Liu et al., 2020a). The reporter plasmid of firefly luciferase (pFLuc) was kindly provided by Dr. Youming Zhang, Shandong University, China.

2.2. Pseudoknot prediction and minigenome construction

Referring to the literature (Willcocks et al., 2011), a putative pseudoknot within SVA IRES was schematically illustrated in Fig. 1. The predicted secondary structure of PKS-II (Fig. 1, dashed yellow rectangle) was formed upon 5-nt-pairing of a single-stranded region in the loop to a stretch of complementary nucleotides. The SVA CH-LX-01–2016 (GenBank: KX751945.1) (Zhao et al., 2017) as a reference strain was modified for constructing the wild-type SVA minigenome, named M0. Briefly, its polyprotein cDNA sequence was replaced with the ORF of NanoLuc® luciferase (NLuc) (Genbank: JQ513379). The minigenome sequence was flanked by the T7 promoter and the T7 terminator at its 5′ and 3′ ends, respectively. The terminal-modifying M0 sequence was chemically synthesized and then subcloned between the *Aat* II and *Afl* III sites of pUC57 plasmid.

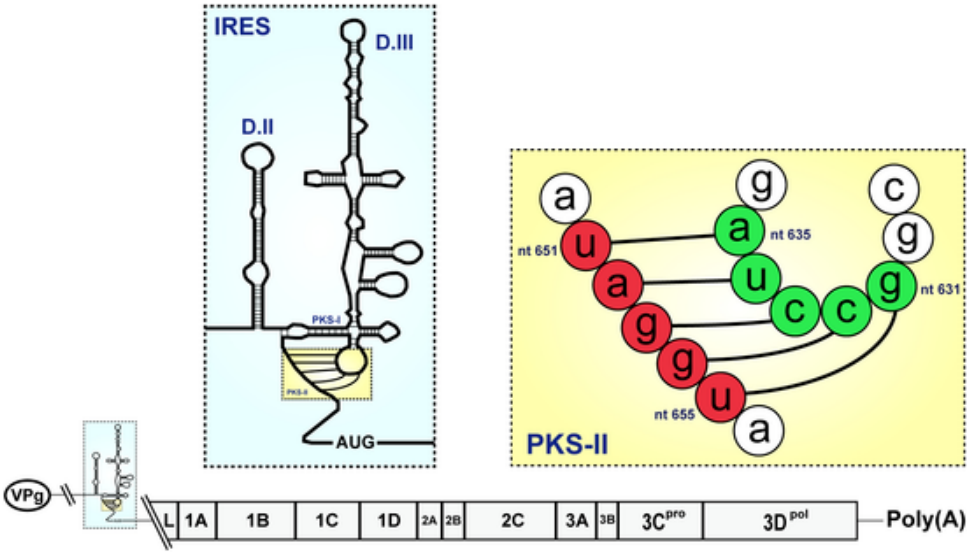

Fig. 1. Schematic representation of putative PKS-II within internal ribosome entry site (IRES) of SVA (CH-LX-01-2016) genome. Proposed secondary structure of IRES (dashed light-blue rectangle), referring to that of the prototype strain (SVV-001) (Willcocks et al., 2011). The predicted secondary structure of PKS-II (dashed yellow rectangle) is formed upon 5-nt-pairing of a single-stranded region in the loop to a stretch of complementary nucleotides. D.II and D.III: Domain II and Domain III; PKS-I and PKS-II: pseudoknot stem I and pseudoknot stem II. (For interpretation of the references to colour in this figure legend, the reader is referred to the web version of this article).

2.3. Kinetics of NLuc expression

BSR-T7/5 cells were plated into four 24-well plates for incubation at 37 °C overnight. Cell monolayers at 70 % confluency were separately transfected with the M0 (100 ng/well, and 3 wells/plate), using Lipofectamine 2000 (Thermo Fisher, Waltham, MA, USA) according to the manufacturer's instruction. At 0, 24, 48 and 72 h post transfection (hpt), any of plates was randomly removed from the incubator, and subjected to two freeze-and-thaw cycles to collect supernatants. All supernatants were separately diluted 100-fold with PBS in a white 96-well plate for measuring their luminescence intensities (with substraction of autoluminescence background) using the Nano-Glo® Luciferase Assay System (Promega, Madison, WI) by the Tecan microplate reader. Kinetic curve of NLuc expression was determined using the GraphPad Prism software (Version 7.0). Data at each time point were representative of three independent experiments.

2.4. Site-directed mutagenesis of PKS-II

The M0 contained two key motifs, 5′-GCCTA-3′ (Fig. 2A, Green-shaded) and 5′-TAGGT-3′ (Fig. 2A, Red-shaded), both of which jointly contributed to the formation of PKS-II. The latter one was subjected to all possible point mutations by site-directed mutagenesis (SDM): five 1-nt-SDMs, ten 2-nt-SDMs, ten 3-nt-SDMs, five 4-nt-SDMs and one 5-nt-SDM. All thirty-one mutants were constructed using the M0 as a template. Briefly, the M0 was subjected to PCR reactions independently using thirty-one pairs of SDM primers (Table 1). The PCR reaction contained 2 × PrimeSTAR Max Premix (Takara, Dalian, China) and underwent 32 cycles at 98 °C (10 s), 58 °C (5 s) and 72 °C (38 s). The PCR product was detected by agarose gel electrophoresis, and then digested with *Dpn* I (Takara, Dalian, China) to degrade the circular plasmid template. The *Dpn* I-digested product was transformed into *E. coli* JM109 competent cells, subsequently incubated on an ampicillin-containing agar plate overnight at 37 °C. Single colonies were inoculated into individual culture tubes for incubation with shaking at 37 °C. All thirty-one mutants were confirmed by Sanger sequencing, and purified using a Mini Plasmid Kit (TIANGEN, Beijing, China) according to the manufacturer's instruction.

2.5. Dual-luciferase reporter assay

BSR-T7/5 cells were plated into 24-well plates for incubation at 37 °C overnight. All mutants and the M0 were separately co-transfected with the pFLuc into cell monolayers at 70 % confluency (Mutants, M0 or pFLuc: 300 ng/well), using Lipofectamine 2000 (Thermo Fisher, Waltham, MA, USA) according to the manufacturer's instruction. At 48 hpt, the 24-well plates were subjected to two freeze-and-thaw cycles to collect supernatants for dual-luciferase reporter assay on NLuc and FLuc intensities using the Nano-Glo® Luciferase Assay System (Promega, Madison, WI) and the Firefly Luciferase Reporter Gene Assay Kit (Beyotime, Shanghai, China), respectively. Luminescence intensities were measured as described in Subheading 2.3. The GraphPad Prism software (Version 7.0) was used for assessing the difference of luminescence intensity ratio (NLuc/FLuc) between the M0 and each mutant by two-tailed Student's *t*-test. The data shown are the means ± standard deviations (SD) of three independent experiments. Statistical significance: $*p < 0.05$, $**p < 0.01$ and $***p < 0.001$.

2.6. Rescue of PKS-II-disrupting rSVA-eGFP

The rSVA-eGFP cDNA clone (Liu et al., 2020a) was used for constructing a mutated plasmid, rSVA-eGFP-M cDNA clone, in which the key pseudoknot-forming motif, 5′-TAGGT-3′, was replaced with its compensatory one, 5′-ATCCG-3′ (Fig. 5A, Red-shaded). The rSVA-eGFP-M cDNA clone was purified for Sanger sequencing to confirm its full-length sequence, and subsequently transfected into BSR-T7/5 cells in an attempt to rescue a competent recombinant virus, rSVA-eGFP-M. Briefly, BSR-T7/5 cells were seeded into a 12-well plate for incubation at 37 °C overnight. One cell monolayer at 70 % confluency was transfected with the rSVA-eGFP-M (2000 ng/well), using Lipofectamine 2000 (Thermo Fisher, Waltham, MA, USA) according to the manufacturer's instruction. At 72 hpt, the 12-well plate was subjected to one freeze-and-thaw cycle to collect supernatant (passage-0, P0) for three serial blind passages, regardless of whether the rSVA-eGFP-M was successfully recovered from its cDNA clone. The rSVA-eGFP cDNA clone was simultaneously transfected for rescuing the non-mutated rSVA-eGFP as a control.

2.7. RT-PCR identification of virus recovery

The passage-3 (P3) rSVA-eGFP-M was harvested for extracting viral RNA by a Viral RNA/DNA Extraction Kit (Takara, Dalian, China). The extracted product was used as template for one-step RT-PCR analysis using the F1/R1 primers for amplifying a 693-bp fragment, as described previously (Liu et al., 2020a). Briefly, the one-step RT-PCR underwent 45 °C for 10 min, 94 °C for 2 min and then 30 cycles at 98 °C (10 s), 55 °C (15 s) and 68 °C (10 s). The extracted RNA was simultaneously subjected to PCR analysis using the F1/R1 primers. The PCR reaction contained 2 × PrimeSTAR Max Premix (Takara, Dalian, China) and underwent 30 cycles at 98 °C (10 s), 55 °C (5 s) and 72 °C (10 s). The P3 rSVA-eGFP was also analyzed simultaneously as a control. If the RT-PCR result indicated the failure of rSVA-eGFP-M recov-

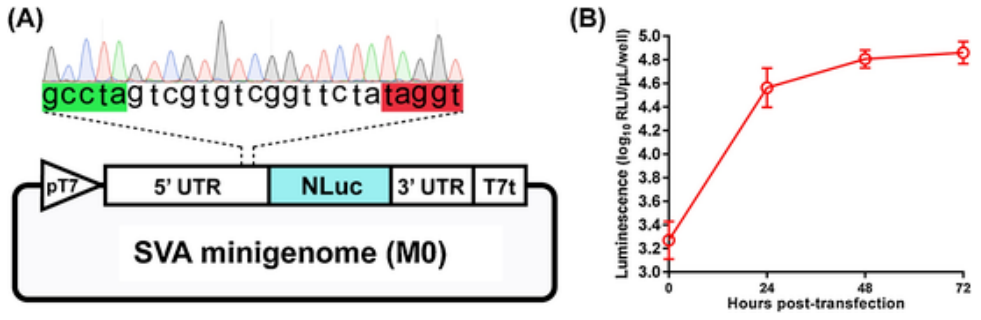

Fig. 2. Construction and characterization of SVA minigenome (M0). Schematic representation of M0 (A). The ORF sequence of SVA polyprotein is replaced with that of the NLuc. The minigenome sequence is flanked by the T7 promoter (pT7) and the T7 terminator (T7t) at its 5′ and 3′ ends, respectively. The sequencing chromatogram illustrates a cDNA fragment, in which two key motifs, 5′-GCCTA-3′ (Green-shaded) and 5′-TAGGT-3′ (Red-shaded), jointly contribute to the formation of pseudoknot stem II. UTR: untranslated region. Kinetic curve of M0-expressed NLuc in BSR-T7/5 cells (B). At 0, 24, 48 and 72 h hpt, M0-transfected cell monolayers are subjected to two freeze-and-thaw cycles to collect supernatants, subsequently diluted 100-fold with PBS for luciferase activity assay in a white 96-well plate using the Tecan microplate reader. The data represent the mean ± SD for three independent experiments. RLU: relative luminescence unit. (For interpretation of the references to colour in this figure legend, the reader is referred to the web version of this article).

Table 1
Primers used for construction of mutated SVA minigenomes by site-directed mutagenesis.

Mutated SVA minigenomes	Forward primers (5′ to 3′)*	Reverse primers (5′ to 3′)*	Mutated PKS-II-forming cDNA sequence#
M1-A	gtcgtgtcggttctaAaggtagcacata	Ttagaaccgacgactaggccgtcgcc	**gcctag**tcgtgtcggttcta**Aaggt**
M1-B	tcgtgtcggttctatTggtagcacatac	Aatagaaccgacacgactaggccgtcgc	**gcctag**tcgtgtcggttcta**tTggt**
M1-C	cgtgtcggttctataCgtagcacataca	Gtatagaaccgacacgactaggccgtcg	**gcctag**tcgtgtcggttcta**taCgt**
M1-D	gtgtcggttctatagCtagcacatacaa	Gctatagaaccgacacgactaggccgtc	**gcctag**tcgtgtcggttcta**tagCt**
M1-E	tgtcggttctataggGagcacatacaaa	Ccctatagaaccgacacgactaggccgt	**gcctag**tcgtgtcggttcta**taggG**
M2-A	tagtcgtgtcggttctaATggtagcacatacaaatatgg	ccatatttgtatgtgctaccATtagaaccgacacgacta	**gcctag**tcgtgtcggttcta**ATggt**
M2-B	tagtcgtgtcggttctaAaCgtagcacatacaaatatgg	ccatatttgtatgtgctacGtTtagaaccgacacgacta	**gcctag**tcgtgtcggttcta**AaCgt**
M2-C	tagtcgtgtcggttctaAagCtagcacatacaaatatgg	ccatatttgtatgtgctaGctTtagaaccgacacgacta	**gcctag**tcgtgtcggttcta**AagCt**
M2-D	tagtcgtgtcggttctaAaggGagcacatacaaatatgg	ccatatttgtatgtgctCcctTtagaaccgacacgacta	**gcctag**tcgtgtcggttcta**AaggG**
M2-E	tagtcgtgtcggttctatTCgtagcacatacaaatatgg	ccatatttgtatgtgctacGAatagaaccgacacgacta	**gcctag**tcgtgtcggttcta**tTCgt**
M2-F	tagtcgtgtcggttctatTgCtagcacatacaaatatgg	ccatatttgtatgtgctaGcAatagaaccgacacgacta	**gcctag**tcgtgtcggttcta**tTgCt**
M2-G	tagtcgtgtcggttctatTggGagcacatacaaatatgg	ccatatttgtatgtgctCccAatagaaccgacacgacta	**gcctag**tcgtgtcggttcta**tTggG**
M2-H	tagtcgtgtcggttctataCCtagcacatacaaatatgg	ccatatttgtatgtgctaGGtatagaaccgacacgacta	**gcctag**tcgtgtcggttcta**taCCt**
M2-I	tagtcgtgtcggttctataCgGagcacatacaaatatgg	ccatatttgtatgtgctCcGtatagaaccgacacgacta	**gcctag**tcgtgtcggttcta**taCgG**
M2-J	tagtcgtgtcggttctatagCGagcacatacaaatatgg	ccatatttgtatgtgctCGctatagaaccgacacgacta	**gcctag**tcgtgtcggttcta**tagCG**
M3-A	tagtcgtgtcggttctaATCgtagcacatacaaatatgg	ccatatttgtatgtgctacGATtagaaccgacacgacta	**gcctag**tcgtgtcggttcta**ATCgt**
M3-B	tagtcgtgtcggttctaATgCtagcacatacaaatatgg	ccatatttgtatgtgctaGcATtagaaccgacacgacta	**gcctag**tcgtgtcggttcta**ATgCt**
M3-C	tagtcgtgtcggttctaATggGagcacatacaaatatgg	ccatatttgtatgtgctCccATtagaaccgacacgacta	**gcctag**tcgtgtcggttcta**ATggG**
M3-D	tagtcgtgtcggttctaAaCCtagcacatacaaatatgg	ccatatttgtatgtgctaGGtTtagaaccgacacgacta	**gcctag**tcgtgtcggttcta**AaCCt**
M3-E	tagtcgtgtcggttctaAaCgGagcacatacaaatatgg	ccatatttgtatgtgctCcGtTtagaaccgacacgacta	**gcctag**tcgtgtcggttcta**AaCgG**
M3-F	tagtcgtgtcggttctaAagCGagcacatacaaatatgg	ccatatttgtatgtgctCGctTtagaaccgacacgacta	**gcctag**tcgtgtcggttcta**AagCG**
M3-G	tagtcgtgtcggttctatTCCtagcacatacaaatatgg	ccatatttgtatgtgctaGGAatagaaccgacacgacta	**gcctag**tcgtgtcggttcta**tTCCt**
M3-H	tagtcgtgtcggttctatTCgGagcacatacaaatatgg	ccatatttgtatgtgctCcGAatagaaccgacacgacta	**gcctag**tcgtgtcggttcta**tTCgG**
M3-I	tagtcgtgtcggttctatTgCGagcacatacaaatatgg	ccatatttgtatgtgctCGcAatagaaccgacacgacta	**gcctag**tcgtgtcggttcta**tTgCG**
M3-J	tagtcgtgtcggttctataCCGagcacatacaaatatgg	ccatatttgtatgtgctCGGtatagaaccgacacgacta	**gcctag**tcgtgtcggttcta**taCCG**
M4-A	tagtcgtgtcggttctatTCCGagcacatacaaatatgg	ccatatttgtatgtgctCGGAatagaaccgacacgacta	**gcctag**tcgtgtcggttcta**tTCCG**
M4-B	tagtcgtgtcggttctaAaCCGagcacatacaaatatgg	ccatatttgtatgtgctCGGtTtagaaccgacacgacta	**gcctag**tcgtgtcggttcta**AaCCG**
M4-C	tagtcgtgtcggttctaATgCGagcacatacaaatatgg	ccatatttgtatgtgctCGcATtagaaccgacacgacta	**gcctag**tcgtgtcggttcta**ATgCG**
M4-D	tagtcgtgtcggttctaATCgGagcacatacaaatatgg	ccatatttgtatgtgctCcGATtagaaccgacacgacta	**gcctag**tcgtgtcggttcta**ATCgG**
M4-E	tagtcgtgtcggttctaATCCtagcacatacaaatatgg	ccatatttgtatgtgctaGGATtagaaccgacacgacta	**gcctag**tcgtgtcggttcta**ATCCt**
M5	tagtcgtgtcggttctaATCCGagcacatacaaatatgg	ccatatttgtatgtgctCGGATtagaaccgacacgacta	**gcctag**tcgtgtcggttcta**ATCCG**

* Mutated nucleotides are shown in uppercase letters.
\# Mutated nucleotides are shown in uppercase letters, and complementary sequences related to PKS-II formation are in bold typeface.

ery, the experiment would be repeated three times to eliminate accidental factors interfering with the rescue of virus.

2.8. Mass spectrometry

The rSVA-eGFP-M cDNA clone was transfected (5000 ng/well) into BSR-T7/5 cells cultured on a 6-well plate, which was subjected to three freeze-and-thaw cycles at 24 hpt to collect supernatant for mass spectrometry at the Shanghai Bioprofile Biotechnology Co., Ltd (Shanghai, China). Briefly, protein digestion was performed with a method of filter-aided sample preparation, as described previously (Wiśniewski et al., 2009). Liquid chromatography linked to tandem mass spectrometry (LC–MS/MS) was performed on a Q Exactive Plus mass spectrometer that was coupled to Easy nLC (Thermo Fisher, Waltham, MA, USA). The MS data were analyzed using MaxQuant software v1.6.0.16. The database search results were filtered and exported with <1% false discovery rate at peptide-spectrum-matched level, and protein level, respectively.

2.9. Analysis of antigenome replication

The rSVA-eGFP-M cDNA clone was transfected (2000 ng/well) into BSR-T7/5 cells cultured on a 12-well plate. The rSVA-eGFP cDNA clone was simultaneously transfected as a control. The plasmid-transfected cells were harvested at 72 hpt for extracting viral RNA by a Viral RNA/DNA Extraction Kit (Takara, Dalian, China). The extracted product was immediately digested with DNase I (Accurate, Changsha, China) to eliminate the cDNA residues that would interfere with the later two-step RT-PCR assay. The DNase I-digested product was used as template for the first-strand cDNA synthesis based on the F2 primer (5′-TGCCAAACTGGGGTATAAGATGA-3′) using the 1 st Strand cDNA Synthesis Kit (Takara, Dalian, China), according to the manufacturer's instruction. The synthesized first-strand cDNA was subsequently used as template for PCR assay based on the F2 and R2 (5′–CCCTTTTCT-GTTCCGACTGAGTT-3′) primers using the PrimeSTAR Max Premix (Takara, Dalian, China), undergoing 35 cycles at 98 °C (10 s), 58 °C (5 s) and 72 °C (5 s). In order to confirm no cDNA residue interfering with the two-step RT-PCR assay, the DNase I-digested product was also used for PCR analysis. The two-step RT-PCR and PCR products were detected by agarose gel electrophoresis, followed by Sanger sequencing for confirming the RT-PCR product.

3. Results

3.1. M0 is constructed for determing kinetic curve of NLuc expression

Fig. 2A showed the M0 map, in which the key pseudoknot-forming motif was marked with its sequencing chromatogram. To examine the kinetics of NLuc expression by the M0 *in vitro*, luciferase activities were measured at each time point after M0 transfection. The kinetic curve showed that 0–24 hpt was an exponential phase of NLuc expression, and the NLuc level remained relatively stable over time after 48 hpt (Fig. 2B).

3.2. M0 is subjected to SDM for constructing PKS-II-disrupting mutants

All thirty-one mutants, five 1-nt-SDMs (M1-A to -E), ten 2-nt-SDMs (M2-A to -J), ten 3-nt-SDMs (M3-A to -J), five 4-nt-SDMs (M4-A to -E) and one 5-nt-SDM (M5), were constructed using the M0 as a template. The SDM PCR-amplified circular products were approximately 3.3 kb in length (Fig. 3A to D). All mutants were subjected to Sanger sequencing for confirming their mutated motifs involved in pseudoknot formation (Fig. 3E).

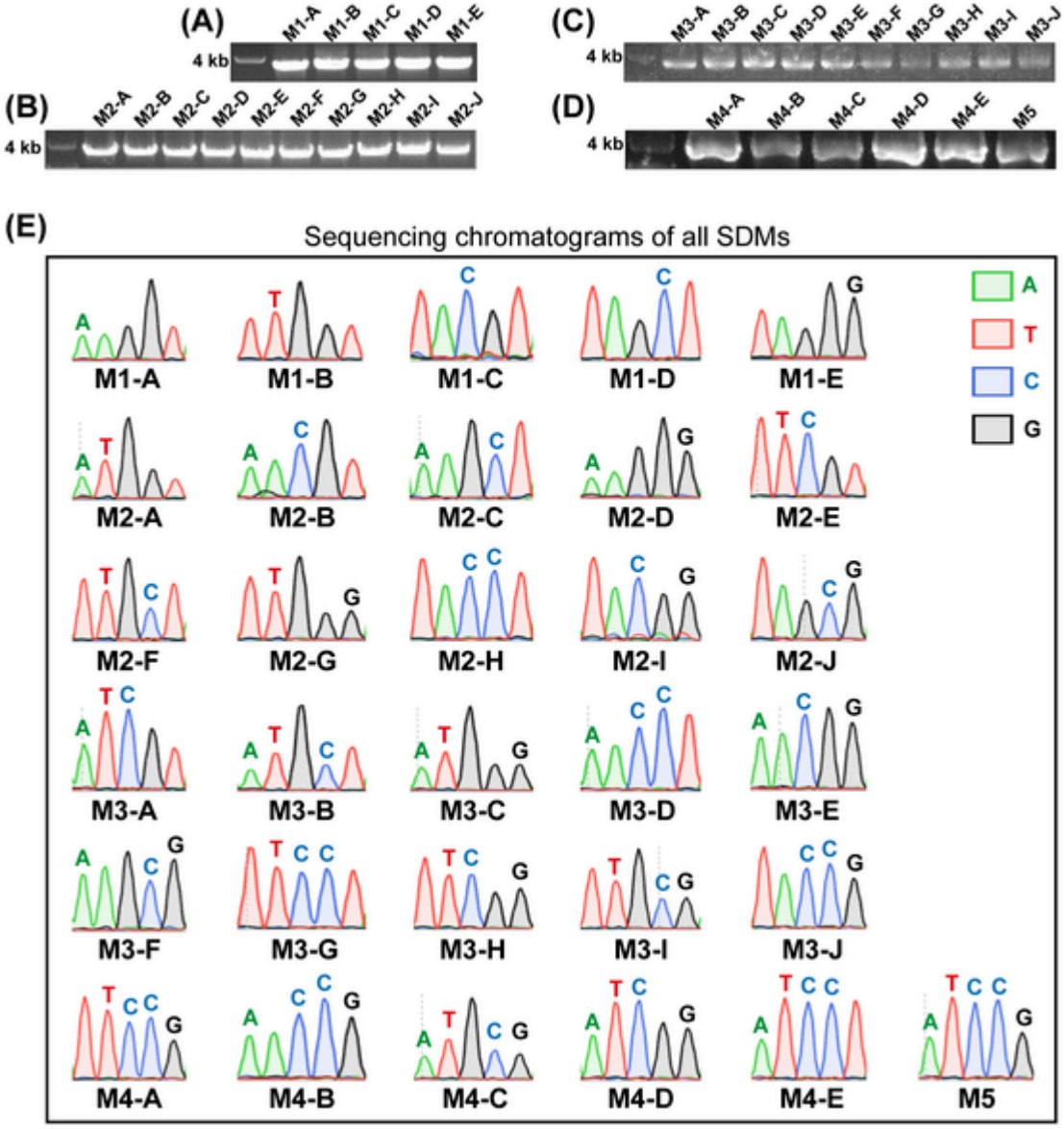

Fig. 3. Site-directed mutageneses (SDM) of a key motif (5′-TAGGT-3′) in M0 contributing to formation of pseudoknot stem II. The original sequence (5′-TAGGT-3′) is subjected to all possible SDMs: five 1-nt-SDMs (A), ten 2-nt-SDMs (B), ten 3-nt-SDMs (C), five 4-nt-SDMs (D) and one 5-nt-SDM (D). All mutated plasmids are confirmed by Sanger sequencing (E). Each mutated nucleotide is marked with A, T, C or G over its chromatogram peak.

3.3. PKS-II-disrupting IRESs do not abolish their abilities to initiate NLuc expression

All mutants were independently co-transfected with the pFLuc into BSR-T7/5 cells for dual-luciferase reporter assays to uncover impacts of point mutations in the PKS-II motif on the NLuc expression. At 48 hpt, both the NLuc and the FLuc could be expressed by each of the mutants at a relatively high level. Both NLuc- and FLuc-based luminescence intensities were more than 10^6 relative luminescence unit (RLU)/well for almost all samples (Fig. 4A). The NLuc/FLuc luminescence intensity ratio (LIR) for each mutant showed that any combination of point mutations could not greatly interfere with the NLuc expression, despite the two-tailed Student′s *t*-test indicating a significant (or extremely significant) difference between the M0 and a given mutant (Fig. 4B). Unexpectedly, some samples, such as the M4-B, -C and -D, showed their LIRs approximately 2-fold higher than that of the M0.

3.4. Recombinant SVA cannot be rescued from 5-nt-mutated cDNA clone

The rSVA-eGFP-M cDNA clone was schematically illustrated in Fig. 5 A. The key pseudoknot-forming motif, 5′-TAGGT-3′, was replaced with its compensatory one, 5′-ATCCG-3′ (Fig. 5A, Red-shaded). After confirmation of its full-length sequence by Sanger sequencing, the rSVA-eGFP-M cDNA clone was transfected into BSR-T7/5 cells in an attempt to rescue a competent rSVA-eGFP-M. At 24 hpt, a small number of cells had begun to emit green fluorescence (Fig. 5B). However, the proportion of fluorescence-emitting cells was not rising over time in the rSVA-eGFP-M cDNA clone-transfected cell monolayer (Fig. 5B), in comparison with that in the control group (Fig. 5C). The rSVA-eGFP-M was subjected to three serial passages in BSR-T7/5 cells, nevertheless showing no green fluorescence during passaging (Fig. 5D). In contrast, the rSVA-eGFP could effectively express the eGFP during serial passages (Fig. 5E).

The P3 rSVA-eGFP-M and rSVA-eGFP were separately harvested for extracting total RNAs, which as templates were used for one-step RT-

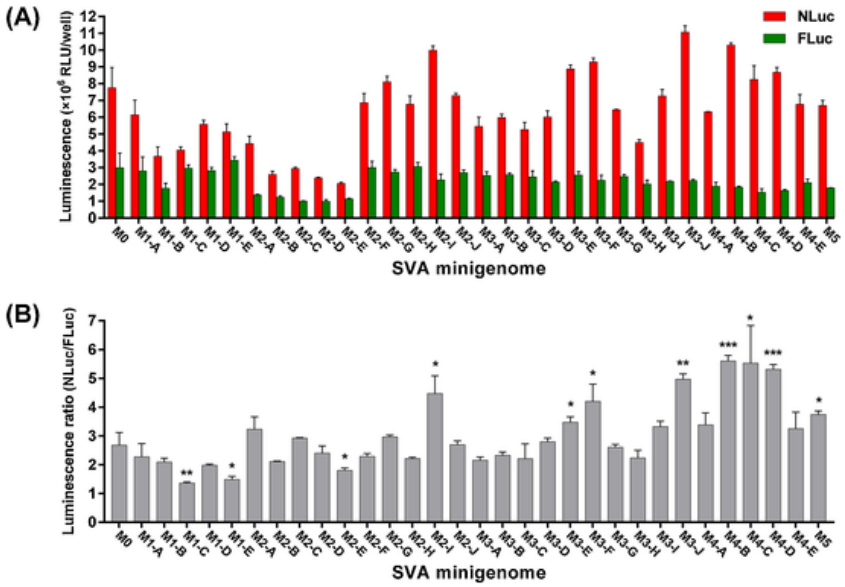

Fig. 4. Dual-luciferase reporter assays for BSR-T7/5 cells co-transfected with pFLuc and mutated SVA minigenome (or M0). Absolute luminescence intensities of NLuc and FLuc for the M0 and all mutants (A). Luminescence intensity ratios (NLuc/FLuc) for the M0 and all mutants (B). At 48 hpt, BSR-T7/5 cells are subjected to two freeze-and-thaw cycles to collect supernatants. Each undiluted supernatant is independently subjected to dual-luciferase reporter assays on NLuc and FLuc. The GraphPad Prism software (Version 7.0) is used for assessing the difference of luminescence intensity ratio (NLuc/FLuc) between the M0 and each mutant by two-tailed Student's *t*-test. The data shown are the means ± SD of three independent experiments. Statistical significance: $*p < 0.05$, $**p < 0.01$ and $***p < 0.001$. RLU: relative luminescence unit.

PCR and PCR analyses. Only the P3 rSVA-eGFP showed an expected 693-bp product, amplified by the one-step RT-PCR (Fig. 5F). The experiment was repeated three times to eliminate accidental factors interfering with the rescue of rSVA-eGFP-M. However, we still observed neither the eGFP expression during passaging, nor the RT-PCR-amplified specific product. Thus, it could be concluded that the 5-nt-mutated cDNA clone interfered with the recovery of recombinant virus.

3.5. The mutated cDNA clone can still initiate expression of interesting proteins

As described in Subheading 3.4., the rSVA-eGFP-M cDNA clone, albeit genetically modified in its theoretically crucial motif for protein expression, could still code for the eGFP as early as 24 hpt or even earlier. In order to explore whether viral self-proteins could also be expressed, the rSVA-eGFP-M cDNA clone was transfected into BSR-T7/5 cells once again, then subjected to three freeze-and-thaw cycles at 24 hpt (Fig. 5G) to collect supernatant for mass spectrometry. The result showed that a total of three unique peptide sequences matched to the MS/MS spectra: ^{42}LLNVIK^{47} in VP1, ^{201}LSSATR^{206} in VP1 and ^{109}TRAEVK^{114} in eGFP (Fig. 5H). The mass spectrometry suggested that the rSVA-eGFP-M cDNA clone could initiate transcription of mRNA (genome) for further protein expression.

3.6. The 5-nt-mutated PKS-II has no impact on antigenome replication

In order to test whether the failure of rSVA-eGFP-M recovery was attributed to inability of antigenome to be replicated from the genome, a pair of specific primers (F2/R2) was designed for two-step RT-PCR to detect the antigenome at P0. The result showed that a 396-bp-specific band only appeared on the RT-PCR lane (Fig. 5I, rSVA-eGFP-M), and the Sanger sequencing revealed the RT-PCR product identical to the 396-bp sequence. The PCR control was simultaneously performed here to reveal no cDNA residue interfering with RT-PCR detection (Fig. 5I, rSVA-eGFP-M). In addition, the P0 rSVA-eGFP exhibited the same RT-PCR and PCR results (Fig. 5I, rSVA-eGFP) as those of the P0 rSVA-eGFP-M. Both RT-PCR and PCR results suggested that the key pseudoknot-forming motif, albeit subjected to five point mutations, had no impact on antigenome replication.

4. Discussion

A picornaviral genome is essentially a non-capped mRNA, and the VPg is covalently linked to its 5′ end. Despite a similar organization of genome among members in the family *Picornaviridae*, their 5′ UTRs still differ in sequence length and in structural element, such as distinct IRESs. Picornaviral IRES element, as a *cis*-acting region, is responsible for recruitment of the ribosomal subunits to initiate translation of viral polyprotein (Lozano and Martínez-Salas, 2015). It has been demonstrated that HCV-like IRESs in members of the *Flaviviviridae* and *Picornaviridae* use the same mechanism to initiate protein expression in an eIF-independent manner: they directly bind to the ribosomal 40S subunit *via* sites that include the GGG motif in domain IIId, domain IIIe, and elements of the pseudoknot (Asnani et al., 2015). The pseudoknot is an indispensable component of HCV-like IRESs. The integrity of PKS-I is critical for binding of the ribosomal 40S subunit. The disruption of PKS-II has been shown to impair IRES's ability to position the start codon in the ribosomal P site (Berry et al., 2010, 2011). The SVA PKS-II is predicted to be a 5-base-paired stem structure (Fig. 1, dashed yellow rectangle). Single or multiple point mutations would possibly inhibit the IRES activity to initiate protein expression.

In this study, in order to explore which single or combined point mutations could totally impair the activity of SVA IRES, we constructed a set of plasmid-based SVA minigenomes, including all single and combined point mutations in one strand of PKS-II. The M0 was a wild-type minigenome, in which the polyprotein ORF was replaced with that of the NLuc. The NLuc is a novel luciferase, approximately 150-fold brighter than others, and has been used as an ideal reporter to rescue recombinant SVA in our previous study (Liu et al., 2021b). Moreover, the NLuc ORF (516 bp) is shorter than those of others, therefore shortening the full-length sequence of M0, and furthermore facilitating construction of mutated minigenomes. It has been reported that NLuc and FLuc are suitable for joint use in the dual-luciferase reporter assay (Germain-Genevois et al., 2016). Therefore, we used the NLuc-inserting minigenomes and the pFLuc for the dual-luciferase reporter assay. Be-

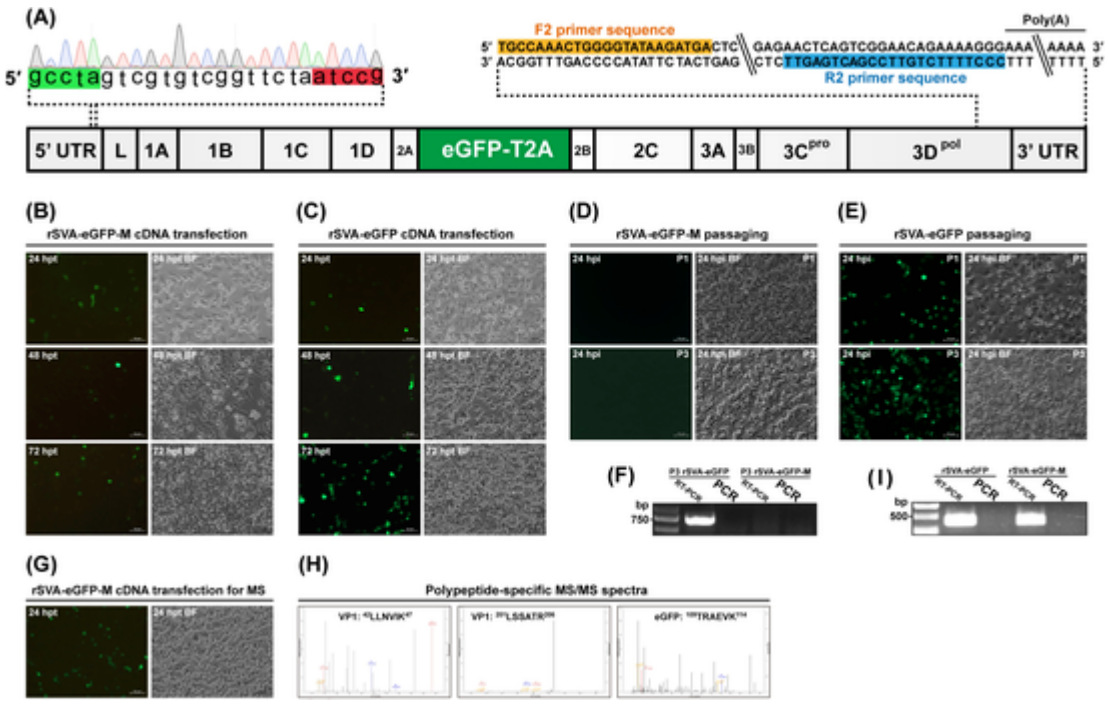

Fig. 5. Impacts of 5-nt-mutated motif related to PKS-II formation on SVA recovery, protein expression and antigenome replication. Schematic representation of 5-nt-mutated rSVA-eGFP-M cDNA clone (A). A putative pseudoknot cannot be formed, due to the absence of complementary base-pairing between 5′-GCCUA-3′ (Light-green-shaded) and 5′-AUCCG-3′ (Red-shaded). The cDNA fragment related to PKS-II formation is illustrated with its sequencing chromatogram. BSR-T7/5 cell monolayers independently transfected with the rSVA-eGFP-M (B) and the rSVA-eGFP (C) cDNA clones. At 72 hpt, two cell monolayers are independently subjected to one freeze-and-thaw cycle to collect supernatants for three serial blind passages, regardless of whether recombinant SVAs are successfully recovered from their cDNA clones. Serial blind passages of rSVA-eGFP-M (D) and rSVA-eGFP (E) in BSR-T7/5 cells. One-step RT-PCR analyses of rSVA-eGFP and rSVA-eGFP-M at P3 using the F1/R1 primer pair (F). Two PCR controls are assigned to reveal no interference of cDNA residues. BSR-T7/5 cell monolayer transfected with rSVA-eGFP-M at 24 hpt (G) for mass spectrometry. Three MS/MS spectra (H), to which three unique peptide sequences match. Two-step RT-PCR analyses of antigenome replication on rSVA-eGFP and rSVA-eGFP-M at 72 hpt using the F2/R2 primer pair (I). The F2 and R2 primers are marked with orange and blue rectangles, respectively (A). The DNase I-digested product is used as template for the first-strand cDNA synthesis only using the F2 primer. The first-strand cDNA serves as template for PCR assay based on the F2/R2 primers. To confirm no cDNA residue interfering with the two-step RT-PCR assay, the DNase I-digested product is also subjected to PCR assay using the F2/R2 primers. (For interpretation of the references to colour in this figure legend, the reader is referred to the web version of this article).

fore the present study, we had constructed a single dicistronic reporter vector, and attempted to use it as a tool for dual-luciferase reporter assay. Our single dicistronic reporter vector followed the standard "promoter–reporter I–5′ UTR–reporter II–terminator" layout. Unfortunately, we found that only the report I was expressed. The failure of report II expression would be attributed to disruption of SVA IRES structure, most possibly by the long RNA sequence upstream of the 5′ UTR.

The dual-luciferase reporter assay in this study demonstrated that any of single or multiple point mutations in PKS-II could not significantly impair the IRES activity for initiating protein expression. Such a result was contrary to that of the literature (Willcocks et al., 2011), which revealed that only two adjacent mutated sites (CC→GG) in the PKS-II could severely inhibit the SVA (SVV-001) IRES activity by analysis of dicistronic reporter construct in 293 T cells. Interestingly, the two adjacent mutated sites were located at one strand (Fig. 1, "gccua"), whereas all mutations in our study targeted its complementary strand (Fig. 1, "uaggu"). In order to unify the mutated sites, the M0 was subsequently subjected to SDM to construct another minigenome (M6) with the two adjacent mutated sites (CC→GG) in the strand of "gccua". However, we found that the M6, like other mutants in this study, still could not inhibit the IRES activity, as evidenced by the dual-luciferase reporter assay (data not shown).

Unexpectedly, there were eight minigenomes (M2-I, M3-E, M3-F, M3-J, M4-B, M4-C, M4-D and M5) with LIRs notably higher than that of the M0 (Fig. 4B). These unexpected results might be attributed to the random errors, because a total of thirty-two minigenomes were transfected and analyzed in different batches. In addition, despite significant (or extremely significant) differences between the M0 and other three minigenomes (M1-C, M1-E and M2-E) (Fig. 4B), the "significant (or extremely significant) difference" was a merely statistical concept, and might result from the random errors as well. Actually, the NLuc expression was not inhibited towards an acceptable level by these three minigenomes (Fig. 4A and B). Indeed, all mutant samples, when mixed with the furimazine substrate, emitted light-blue luminescence that was visible in a darkroom.

According to the results in Fig. 4, we hypothesized that a PKS-II-disrupting SVA IRES is unable to interfere with viral characteristics, such as replication, packaging and infectivity. In order to test our hypothesis, the rSVA-eGFP cDNA clone was subjected to SDM to construct the rSVA-eGFP-M cDNA clone, subsequently transfected into BSR-T7/5 cells in attempting to rescue a competent SVA. The green fluorescence was visible at 24 hpt (Fig. 5B), implying that the 5-nt-mutated motif had no significant impact on the expression of polypeptide or at least eGFP. The following mass spectrometry revealed several peptide sequences, which matched to SVA polypeptide but were also identified in the cell database (data not shown). Eliminating all of these non-specific peptide sequences, we screened out three unique ones that specifically matched to the rSVA-eGFP-M polypeptide. Compared with our previous report (Liu et al., 2021a), in which the SVA-infected cell culture showed a total of thirteen unique peptides, the present study only identified three unique ones *via* mass spectrometry, due to the plasmid-expressed polypeptide at a low level in cells at 24 hpt.

The co-expression of eGFP and VP1 (Fig. 5B, G and H) indirectly demonstrated that mRNA, or positive-sense SVA genome, could be

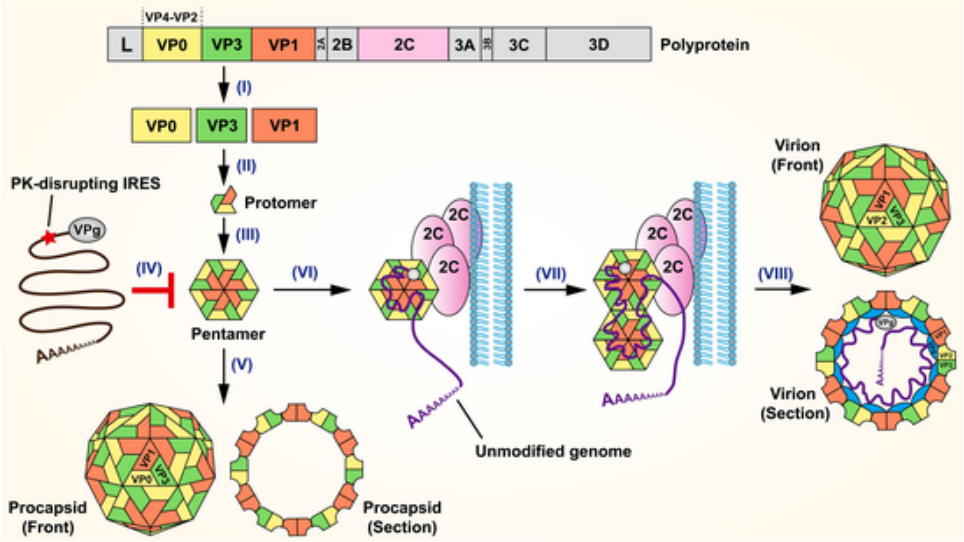

Fig. 6. Hypothesized model of failure in SVA morphogenesis due to PKS-II-disrupting genome, compared with encapsidation of wild-type SVA genome to form infectious virion. The schematic representation is created *via* known aspects of picornavirus morphogenesis (Jiang et al., 2014; Shakeel et al., 2017; Strauss et al., 2018). The polyprotein precursor is expressed, and then undergoes proteolytic processing to release VP0, VP1 and VP3 (I), all of which interact to one another to form a protomer (II). Five protomers assemble to generate a pentamer (III). A PKS-II-disrupting genome cannot interact with the pentamer, possibly attributed to a packaging signal disturbed for RNA encapsidation (IV). Twelve pentamers, albeit deficient in interaction with a complete genome, can self-assemble to generate a procapsid but with low efficiency (V). One pentamer is recruited to the replication complex to interact with a VPg-linked genome without genetic modification (VI). The nonstructural protein, 2C, plays a key role in morphogenesis. As each protomer binds RNA, the genome would form a loop until the next sequence of packaging signal appears (VII). Twelve pentamers condense around the RNA to produce a noninfectious provirion, and subsequently the VP0 is cleaved into VP4 and VP2, finally forming a mature virion (VIII).

transcripted from the rSVA-eGFP-M cDNA clone. In general, RNA replication of picornaviruses (*e.g.*, poliovirus) requires genome circularization through a protein–protein bridge (Herold and Andino, 2001). The 5′ and 3′ ends of viral RNA interact to form a circular ribonucleoprotein complex that regulates the stability, translation and replication of poliovirus RNA (Barton et al., 2001). In the present study, it is unclear whether the mRNA can serve as a template for replication of the antigenome, due to a 5-nt-mutated motif upstream of the start codon. Therefore, we designed the two-step RT-PCR for specific detection of the SVA antigenome using the F2 and R2 primers. It should be noted that the R2 primer must be designed to anneal to its complementary sequence that is closely adjacent to the poly (A) tail, in order to ensure the specific detection of SVA antigenome. The result of two-step RT-PCR indicated the replication of antigenome (Fig. 5I), which was not inhibited by the disruption of PKS-II.

Although PKS-II-disrupting IRES interfered neither with protein expression nor with antigenome replication, we found that competent rSVA-eGFP-M could not be rescued from its cDNA clone. The rSVA-eGFP-M cDNA clone was approximately 8 kb in length. Such a long sequence might harbor lethal mutated sites that would inhibit recovery of virus. To exclude this possibility, the full-length rSVA-eGFP-M cDNA clone was subjected to Sanger sequencing, consequently revealing no unwanted mutation in it (data not shown). We attempted to rescue the rSVA-eGFP-M for three times, but were unsuccessful. We propose one possibility that the PKS-II-disrupting event inhibits encapsidation of SVA genome so that the competent virus can not be rescued, because the encapsidation of picornaviral genome is an indispensable step in recovery of recombinant virus.

In general, selective encapsidation of a picornaviral genome, neither cellular RNAs nor a viral antigenome, requires the specific recognition of packaging signals, which generally are sequences and (or) structures unique to viral nucleic acid. For example, electron microscopy showed that RNA replication complexes of poliovirus co-localized with capsid precursors on membranous vesicles during infection (Pfister et al., 1992). Aichi virus (picornavirus) was reported to contain a 5′-end sequence critical for viral RNA encapsidation (Sasaki and Taniguchi, 2003). Human parechovirus was recently shown to depend on genomic RNA folding to mediate its morphogenesis (Shakeel et al., 2017). Deficits in encapsidation for modified viruses are likely to arise from the elimination of essential interaction between a genome and capsid proteins (Chandler-Bostock et al., 2020).

Based on known aspects of picornavirus morphogenesis (Jiang et al., 2014; Shakeel et al., 2017; Strauss et al., 2018), we propose one hypothesized model (Fig. 6) to exhibit how the PKS-II-disrupting genome cannot be encapsidated, in comparison with how an unmodified genome is packaged into the capsid to form an infectious virion. A classical theory of packaging signal assumes the presence of a single site of packaging signal with affinity for cognate coat protein, consequently forming an assembly initiation complex of RNA-coat protein for further encapsidation (Shakeel et al., 2017). Our hypothesized model supposes that a PKS-II-disrupting genome would lose its packaging signal, and therefore cannot interact with a pentamer or (and) other key factors, such as the 2C protein, finally causing encapsidation failure. It was recently demonstrated that enterovirus assembly depended on multiple and conserved contacts between genomic RNA and coat protein (Chandler-Bostock et al., 2020). We did not demonstrate here that the PKS-II was a packaging signal for SVA. If so, it would likely be one of the multiple packaging signals. Besides the consideration of PKS-II-based packaging signal, there may be other factors responsible for the failure of rSVA-eGFP-M recovery.

Declaration of Competing Interest

The authors report no declarations of interest.

Acknowledgements

This work was supported by the National Key R&D Program for the 13th Five-Year Plan, China (2016YFD050110404), and the Research Foundation for Distinguished Scholars of Qingdao Agricultural University (1120045), China. We thank Dr. Youming Zhang, Shandong University, for offering the pFLuc to us.

References

Asnani, M., Kumar, P., Hellen, C.U., 2015. Widespread distribution and structural diversity of Type IV IRESs in members of Picornaviridae. Virology 478, 61–74.

Bakhshesh, M., Groppelli, E., Willcocks, M.M., Royall, E., Belsham, G.J., Roberts, L.O., 2008. The picornavirus avian encephalomyelitis virus possesses a hepatitis C virus-like internal ribosome entry site element. J. Virol. 82, 1993–2003.

Barton, D.J., O'Donnell, B.J., Flanegan, J.B., 2001. 5' cloverleaf in poliovirus RNA is a cis-acting replication element required for negative-strand synthesis. EMBO J. 20, 1439–1448.

Belsham, G.J., 2009. Divergent picornavirus IRES elements. Virus Res. 139, 183–192.

Berry, K.E., Waghray, S., Doudna, J.A., 2010. The HCV IRES pseudoknot positions the initiation codon on the 40S ribosomal subunit. RNA 16, 1559–1569.

Berry, K.E., Waghray, S., Mortimer, S.A., Bai, Y., Doudna, J.A., 2011. Crystal structure of the HCV IRES central domain reveals strategy for start-codon positioning. Structure 19, 1456–1466.

Boehringer, D., Thermann, R., Ostareck-Lederer, A., Lewis, J.D., Stark, H., 2005. Structure of the hepatitis C virus IRES bound to the human 80S ribosome: remodeling of the HCV IRES. Structure 13, 1695–1706.

Brierley, I., Pennell, S., Gilbert, R.J., 2007. Viral RNA pseudoknots: versatile motifs in gene expression and replication. Nat. Rev. Microbiol. 5, 598–610.

Buchholz, U.J., Finke, S., Conzelmann, K.K., 1999. Generation of bovine respiratory syncytial virus (BRSV) from cDNA: BRSV NS2 is not essential for virus replication in tissue culture, and the human RSV leader region acts as a functional BRSV genome promoter. J. Virol. 73, 251–259.

Chandler-Bostock, R., Mata, C.P., Bingham, R.J., Dykeman, E.C., Meng, B., Tuthill, T.J., Rowlands, D.J., Ranson, N.A., Twarock, R., Stockley, P.G., 2020. Assembly of infectious enteroviruses depends on multiple, conserved genomic RNA-coat protein contacts. PLoS Path. 16, e1009146.

Chard, L.S., Bordeleau, M.E., Pelletier, J., Tanaka, J., Belsham, G.J., 2006a. Hepatitis C virus-related internal ribosome entry sites are found in multiple genera of the family Picornaviridae. J. Gen. Virol. 87, 927–936.

Chard, L.S., Kaku, Y., Jones, B., Nayak, A., Belsham, G.J., 2006b. Functional analyses of RNA structures shared between the internal ribosome entry sites of hepatitis C virus and the picornavirus porcine teschovirus 1 Talfan. J. Virol. 80, 1271–1279.

Easton, L.E., Locker, N., Lukavsky, P.J., 2009. Conserved functional domains and a novel tertiary interaction near the pseudoknot drive translational activity of hepatitis C virus and hepatitis C virus-like internal ribosome entry sites. Nucleic Acids Res. 37, 5537–5549.

Germain-Genevois, C., Garandeau, O., Couillaud, F., 2016. Detection of brain tumors and systemic metastases using NanoLuc and fluc for dual reporter imaging. Mol. Imaging Biol. 18, 62–69.

Hales, L.M., Knowles, N.J., Reddy, P.S., Xu, L., Hay, C., Hallenbeck, P.L., 2008. Complete genome sequence analysis of Seneca Valley virus-001, a novel oncolytic picornavirus. J. Gen. Virol. 89, 1265–1275.

Herold, J., Andino, R., 2001. Poliovirus RNA replication requires genome circularization through a protein-protein bridge. Mol. Cell 7, 581–591.

Houston, E., Temeeyasen, G., Piñeyro, P.E., 2020. Comprehensive review on immunopathogenesis, diagnostic and epidemiology of Senecavirus A. Virus Res. 286, 198038.

Jang, S.K., Kräusslich, H.G., Nicklin, M.J., Duke, G.M., Palmenberg, A.C., Wimmer, E., 1988. A segment of the 5' nontranslated region of encephalomyocarditis virus RNA directs internal entry of ribosomes during in vitro translation. J. Virol. 62, 2636–2643.

Jiang, P., Liu, Y., Ma, H.C., Paul, A.V., Wimmer, E., 2014. Picornavirus morphogenesis. Microbiol. Mol. Biol. Rev. 78, 418–437.

Kaku, Y., Chard, L.S., Inoue, T., Belsham, G.J., 2002. Unique characteristics of a picornavirus internal ribosome entry site from the porcine teschovirus-1 talfan. J. Virol. 76, 11721–11728.

Kieft, J.S., Zhou, K., Jubin, R., Doudna, J.A., 2001. Mechanism of ribosome recruitment by hepatitis C IRES RNA. RNA 7, 194–206.

Liu, F., Huang, Y., Wang, Q., Shan, H., 2020a. Construction of eGFP-Tagged senecavirus a for facilitating virus neutralization test and antiviral assay. Viruses 12, E283.

Liu, F., Wang, Q., Huang, Y., Wang, N., Shan, H., 2020b. A 5-Year review of senecavirus A in China since its emergence in 2015. Front. Vet. Sci. 7, 567792.

Liu, F., Huang, Y., Wang, Q., Li, J., Shan, H., 2021a. Rescue of Senecavirus A to uncover mutation profiles of its progenies during 80 serial passages in vitro. Vet. Microbiol. 253, 108969.

Liu, F., Wang, Q., Huang, Y., Wang, N., Shan, H., 2021b. Rescue of NanoLuc luciferase-expressing Senecavirus A with oncolytic activity. Virus Res. 292, 198232.

Lozano, G., Martínez-Salas, E., 2015. Structural insights into viral IRES-dependent translation mechanisms. Curr. Opin. Virol. 12, 113–120.

Martínez-Salas, E., Francisco-Velilla, R., Fernandez-Chamorro, J., Lozano, G., Diaz-Toledano, R., 2015. Picornavirus IRES elements: RNA structure and host protein interactions. Virus Res. 206, 62–73.

McKnight, K.L., Lemon, S.M., 2018. Hepatitis a virus genome organization and replication strategy. Cold Spring Harb. Perspect. Med. 8, a033480.

Otto, G.A., Puglisi, J.D., 2004. The pathway of HCV IRES-mediated translation initiation. Cell 119, 369–380.

Pan, M., Yang, X., Zhou, L., Ge, X., Guo, X., Liu, J., Zhang, D., Yang, H., 2012. Duck Hepatitis A virus possesses a distinct type IV internal ribosome entry site element of picornavirus. J. Virol. 86, 1129–1144.

Pelletier, J., Sonenberg, N., 1988. Internal initiation of translation of eukaryotic mRNA directed by a sequence derived from poliovirus RNA. Nature 334, 320–325.

Pfister, T., Pasamontes, L., Troxler, M., Egger, D., Bienz, K., 1992. Immunocytochemical localization of capsid-related particles in subcellular fractions of poliovirus-infected cells. Virology 188, 676–684.

Reddy, P.S., Burroughs, K.D., Hales, L.M., Ganesh, S., Jones, B.H., Idamakanti, N., Hay, C., Li, S.S., Skele, K.L., Vasko, A.J., Yang, J., Watkins, D.N., Rudin, C.M., Hallenbeck, P.L., 2007. Seneca Valley virus, a systemically deliverable oncolytic picornavirus, and the treatment of neuroendocrine cancers. J. Natl. Cancer Inst. 99, 1623–1633.

Sasaki, J., Taniguchi, K., 2003. The 5'-end sequence of the genome of Aichi virus, a picornavirus, contains an element critical for viral RNA encapsidation. J. Virol. 77, 3542–3548.

Shakeel, S., Dykeman, E.C., White, S.J., Ora, A., Cockburn, J.J.B., Butcher, S.J., Stockley, P.G., Twarock, R., 2017. Genomic RNA folding mediates assembly of human parechovirus. Nat. Commun. 8, 5.

Strauss, M., Jayawardena, N., Sun, E., Easingwood, R.A., Burga, L.N., Bostina, M., 2018. Cryo-electron microscopy structure of Seneca Valley virus procapsid. J. Virol. 92, e01927-1917.

Sun, D., Chen, S., Cheng, A., Wang, M., 2016. Roles of the picornaviral 3C proteinase in the viral life cycle and host cells. Viruses 8, 82.

Wadhwa, L., Hurwitz, M.Y., Chevez-Barrios, P., Hurwitz, R.L., 2007. Treatment of invasive retinoblastoma in a murine model using an oncolytic picornavirus. Cancer Res. 67, 10653–10656.

Wang, H., Li, Y., 2019. Recent progress on functional genomics research of enterovirus 71. Virol. Sin. 34, 9–21.

Willcocks, M.M., Locker, N., Gomwalk, Z., Royall, E., Bakhshesh, M., Belsham, G.J., Idamakanti, N., Burroughs, K.D., Reddy, P.S., Hallenbeck, P.L., Roberts, L.O., 2011. Structural features of the Seneca Valley virus internal ribosome entry site (IRES) element: a picornavirus with a pestivirus-like IRES. J. Virol. 85, 4452–4461.

Wiśniewski, J.R., Zougman, A., Nagaraj, N., Mann, M., 2009. Universal sample preparation method for proteome analysis. Nat. Methods 6, 359–362.

Zhao, X., Wu, Q., Bai, Y., Chen, G., Zhou, L., Wu, Z., Li, Y., Zhou, W., Yang, H., Ma, J., 2017. Phylogenetic and genome analysis of seven senecavirus A isolates in China. Transbound. Emerg. Dis. 64, 2075–2082.